J Oceanogr (2011) 67:173–182
DOI 10.1007/s10872-011-0016-5

ORIGINAL ARTICLE

Reciprocal sound transmission measurement of mean current and temperature variations in the central part (Aki-nada) of the Seto Inland Sea, Japan

Yudi Adityawarman · Arata Kaneko · Koji Nakano · Naokazu Taniguchi · Katsuaki Komai · Xinyu Guo · Noriaki Gohda

Received: 3 August 2010 / Revised: 9 October 2010 / Accepted: 21 February 2011 / Published online: 12 April 2011

Abstract A 30 km-range reciprocal sound transmission experiment was carried out on the line connecting Honshu and Shikoku (the first and fourth biggest main Japanese islands, respectively) in the central part (Aki-nada) of the Seto Inland Sea, Japan, during March–May 2010 to measure the mean current and temperature variations over the sea. The range-averaged current along the sound transmission line was estimated to have a mean and standard deviation of (3.8–4.4) ± (1.7–1.8) cm/s after converting the travel time difference data into currents, including a fortnightly tidal variation in the range of ±30 cm/s. The positive mean current implies slow water movement from the west to east through Aki-nada. The range-averaged speed of sound was estimated by converting from the mean travel time or one-way travel time into the speed of sound, and further converted into temperature for fixed values of salinity and depth, according to the standard speed of sound formula. Besides the precise measurement (to an accuracy of 0.01°C) of semidiurnal and diurnal tidal variations and seasonal warming, the temperature data showed periodic variations with periods of 7.0 and 21.1 days that had never been observed in Aki-nada before. This study suggests that reciprocal sound transmission is a powerful technique for the long-term accurate measurement of mean current and temperature variations in coastal and inland seas.

Y. Adityawarman · A. Kaneko (✉) · K. Nakano · N. Taniguchi · K. Komai · N. Gohda
Graduate School of Engineering, Hiroshima University, 1-4-1 Kagamiyama, Higashi-Hiroshima 739-8527, Japan
e-mail: akaneko@hiroshima-u.ac.jp

X. Guo
Center for Marine Environmental Studies, Ehime University, 2-5 Bunkyo-cho, Matsuyama 790-8577, Japan

Keywords Aki-nada · Seto Inland Sea · Mean current · Temperature variation · Long-term reciprocal sound transmission experiment

1 Introduction

The Seto Inland Sea is the biggest inland sea in Japan, and is surrounded by three main Japanese islands (Honshu, Kyushu and Shikoku). The east–west length, horizontal area and average depth of the sea are 450 km, 23203 km^2 and 38 m, respectively. Water pollution is present around the urban and industrial regions surrounding the inland sea, and this sometimes leads to disastrous events—such as red tides that damage the fish and oyster aquaculture industries—in a number of places inside the inland sea. However, the environmental problems are confined to rather specific regions around industrial areas; they do not extend over the central regions of the inland sea.

The Seto Inland Sea is connected to the Pacific Ocean through the Bungo Channel and the Kii Channel—located on the southwestern and the southeastern sides of the sea, respectively—and is significantly affected by the Kuroshio, which flowing off both of the channels. Although the Kanmon Strait also represents an outlet to the Sea of Japan at the western edge of the inland sea, its effect on the inland sea may be negligible due to the narrowness of the strait. The near-surface water near the northern front of the Kuroshio enters the Bungo Channel with a mean periodicity of 10 days (warming season) or 8 days (cooling season) as the Kyucho (rapid tides) (Takeoka et al. 1993; Akiyama and Saitoh 1993). On the other hand, the northern part of the Kuroshio surface water enters the Kii Channel as part of the Furiwake-cho (Bifurcation Current) when the Kuroshio is close to the Kii Peninsula (Takeuchi et al. 1998).

Although the Kuroshio intrusions may provide a significant influence on the overall environment of the Seto Inland Sea, little is known about their effect on the central part of the inland sea, in contrast to the Bungo and Kii Channels.

The mean current—in other words the subtidal current—in the Seto Inland Sea has been studied as residual currents in various regions of the inland sea. An overview of the mean current was reported by Yanagi and Higuchi (1979) based on currentmeter data from limited periods of a few days. However, these data were not sufficient to gauge the long-term variations in the mean current in a specified region. Most recent studies have been based on numerical models (Guo et al. 2004; Arai 2004; Chang et al. 2009), and observational data have been acquired in only limited areas due to the difficulty involved in acquiring such data when fisheries are active (Takasugi et al. 1994a, b). It has been proposed that the mean currents through the inland sea are generated by the pressure gradient between the western and eastern parts of the inland sea (Kunii and Fujiwara 2006) or between the Bungo and Kii Channels at the outlets to the Pacific Ocean (Komai et al. 2008a). It has also been reported that density differences produced in the inland sea by Kuroshio intrusion cause the movement of inland sea water (Komai et al. 2008b). However, the mean currents have never been validated by direct observations, as this is a rather difficult task.

The coastal acoustic tomography system (CATS), which has been developed by Hiroshima University as an application of deep-sea acoustic tomography (Munk et al. 1995), and was shown to operate effectively in the coastal seas around Japan, is a large step towards solving the above problem (Park and Kaneko 2000; Yamaguchi et al. 2005; Lin et al. 2005; Kaneko et al. 2005; Nguyen et al. 2009). In the present work, the CATS was applied to measure the mean current and temperature variations in the central region (Aki-nada) of the Seto Inland Sea, where considerable tidal currents occur. The mean current through Aki-nada between Honshu and Shikoku must be measured over a long period to remove tidal components from the data over the sea.

2 Experiment

A 30 km-range reciprocal sound transmission experiment was carried out to measure the mean current and temperature variations in the sea between the stations T1 and T2 (distance 30.17 km) at the central part (Aki-nada) of the Seto Inland Sea, Japan, during March–May 2010 (Fig. 1). The mean floor depth was 8 m at T1 and increased monotonically to 33 m at 15 km away from T1. The floor depth reached a maximum of 49 m around 20 km from T1, and suddenly became shallower toward T2, where the mean floor depth was 14 m. The floor depth was over 40 m 16–23 and 25–28 km away from T1, which remained the main traffic route of the inland sea. A CATS was placed at the edge of the breakwater that protects the fishery port, and a 4 kHz acoustic transducer was suspended by rope 2 m from the bottom in front of the offshore side of the breakwater and connected to the CATS via a cable (Fig. 2). Power was supplied to CATS by 12 and 24 V solar batteries.

The transducer (ITC 2002A) was of the broad-band type with a central frequency of 4 kHz and a band width of 1.4 kHz. The transducer can be applied to not only sound transmission but also sound reception. The source level of the broad-band transducer was 192 dB re 1 μPa at 1 m, and the average power consumption was 480 W during sound transmission. In this experiment, the transmitted signal was phase-modulated by a twelfth-order M sequence to increase the signal-to-noise ratio (SNR) of the received signals by $20\log\sqrt{2^{12}-1} = 36$ dB. This gain in SNR was attained by cross-correlating the received signals with the M sequence used in transmission. Three cycles per digit was selected to transmit the phase-modulated sound from the broad-band transducer. The transmission of 4 kHz sound at 3 cycles per digit requires a frequency bandwidth of 4 kHz/3 = 1.3 kHz, which the present transducer satisfied. The time resolution for multi-arrivals (one-digit width of the M sequence) was 0.75 ms. Six repeated periods of sound (18.43 s), phase-modulated by the M sequence, were released every 15 min upon synchronized timing from T1 and T2. Repeat transmission was also devised to increase the SNR by $20\log\sqrt{N}$ dB (N: repeat number) through an ensemble average. The fluctuation in the data received during the six repeated periods of sound provides the short-term accuracy of the system under fixed environmental conditions.

The travel times are identified at the maximum peak point in the correlation waveform received for each of the six repeated periods of sound. The mean travel times for the periods of sound received are used to calculate the range-averaged current and speed of sound, and the standard deviation (STD) from their mean values serves as an index of short-term variations, which is equivalent to an error bar. The travel times for the reciprocal sound transmission between the stations T1 and T2 can be expressed by

$$t_1 = \frac{L}{C_\mathrm{m} + V_\mathrm{m}} \tag{1}$$

$$t_2 = \frac{L}{C_\mathrm{m} - V_\mathrm{m}}, \tag{2}$$

where L denotes the station-to-station distance, and t_1 and t_2 denote the travel times from T1 to T2 and from T2 to T1, respectively. By solving the coupled Eqs. 1 and 2, the

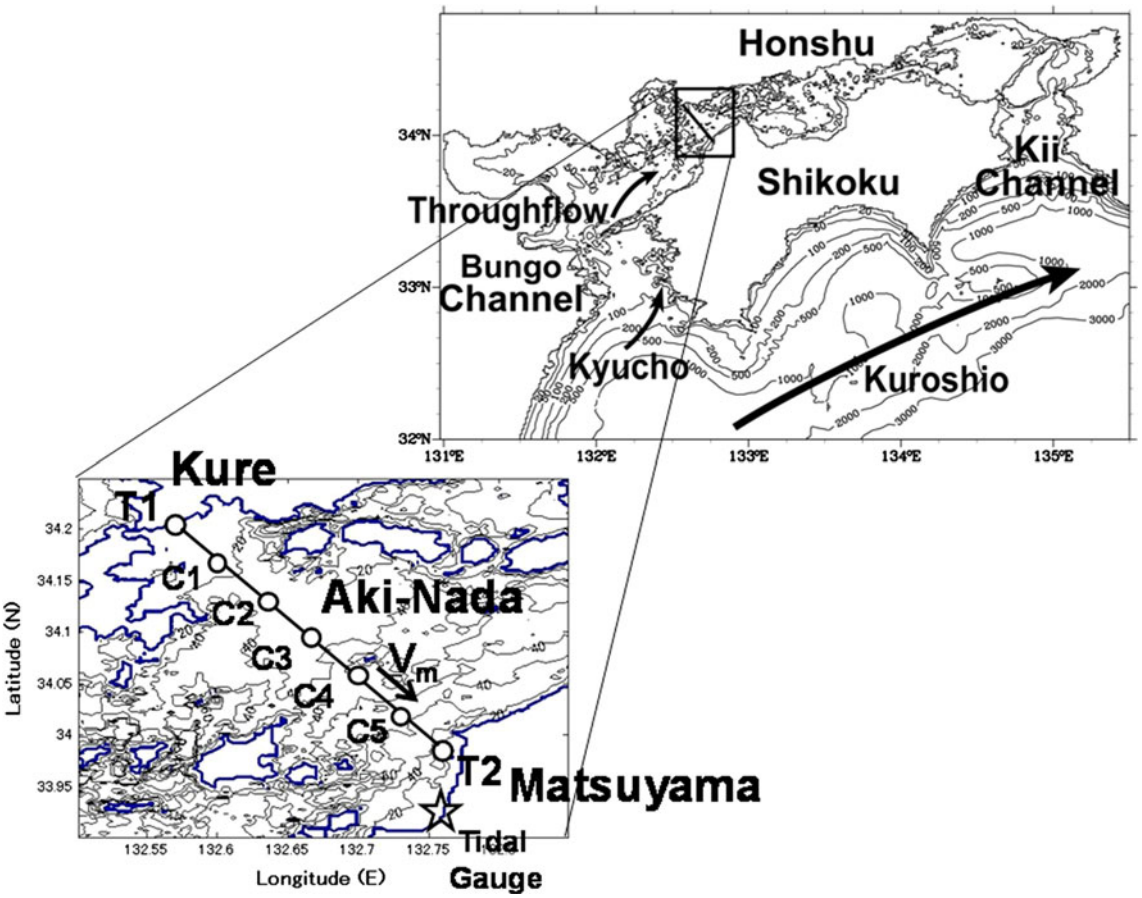

Fig. 1 Map of the location of the experimental site and the surrounding region with a bathymetric chart. The whole region of the Seto Inland Sea is shown on a larger scale in the *upper right* of the figure. *T1* and *T2* are the acoustic stations, and *C1–C5* are the CTD stations. V_m indicates the positive current along the transmission line. The tidal gauge station is indicated by an *asterisk*

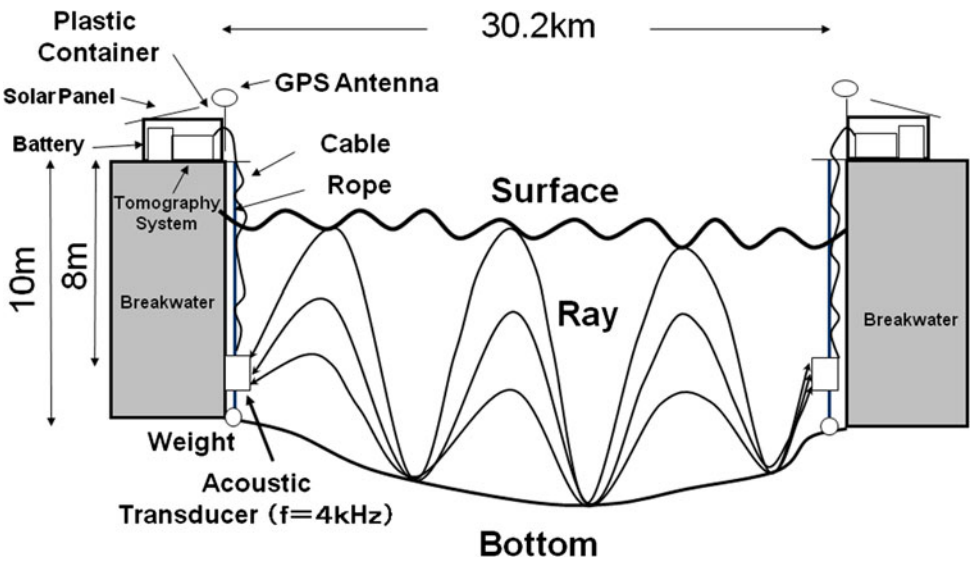

Fig. 2 Schematic diagram of the long-range reciprocal sound transmission experiment located at the breakwater at the fishery port

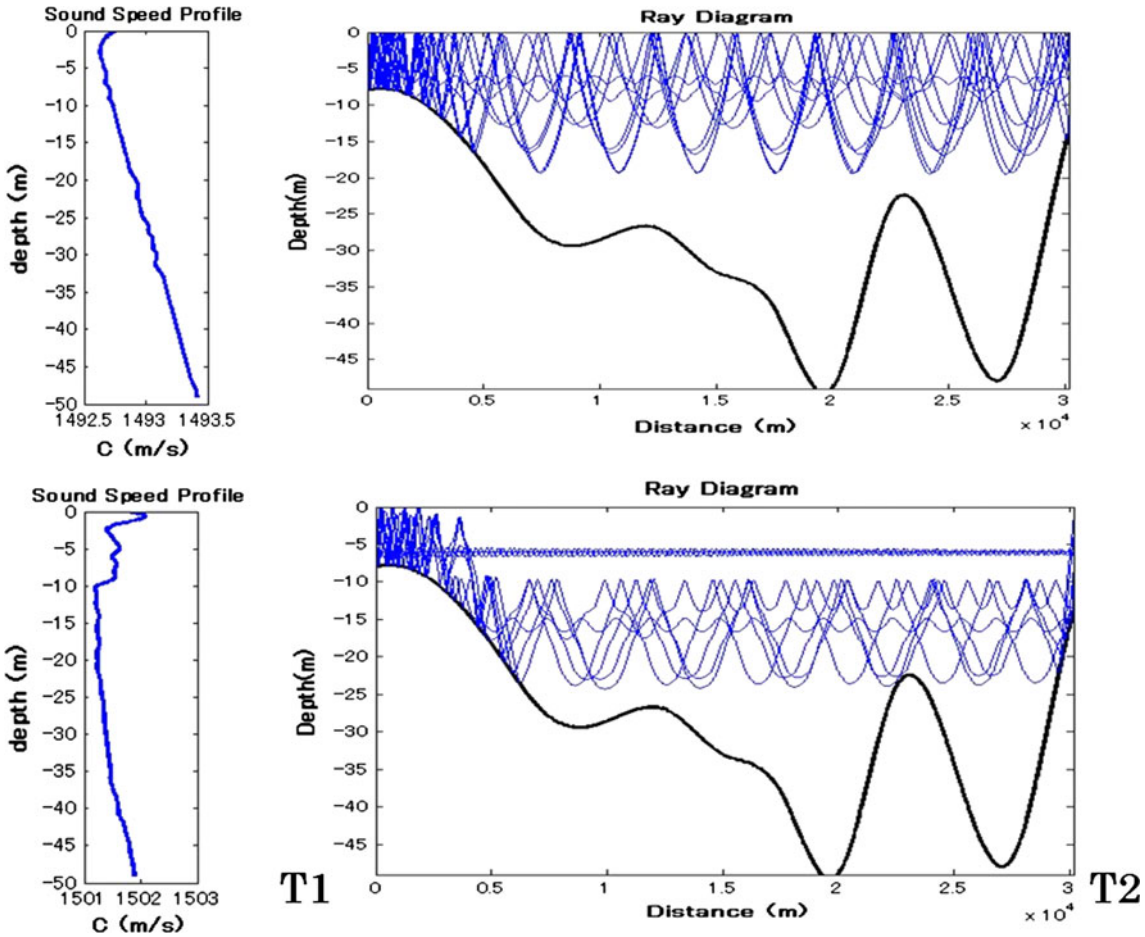

Fig. 3 Results of the range-independent ray simulation using CTD data at C4 (20 km from T1) on March 15 (*upper panel*) and May 12 (*lower panel*). Vertical profiles of the speed of sound (C) are shown on the *left* of the figure

range-average velocity V_m and the speed of sound C_m for the region between the stations T1 and T2 can related to the travel time difference Δt and the mean travel time t_m, respectively, as shown in the following formulae:

$$V_m = \frac{L}{2t_1 t_2}\Delta t \tag{3}$$

$$C_m = \frac{L}{2t_1 t_2} t_m. \tag{4}$$

CTD casts were performed at 5 km intervals on March 15 and May 12 along the sound transmission line. The results were used not only as comparison data in sound transmission measurements but also as data for a range-independent ray-tracing simulation. The results of this range-independent ray simulation for the March and May data are shown in Fig. 3. Here, the speed of sound profile is smoothed using a spline function prior to the simulation. Sound mainly traveled in the upper 20 m for the March data and in the depth range from 10 to 25 m for the May data, because the minimum speed of sound was found to occur at a depth of 2 m in the March data and at a depth of 10 m in the May data when constructing the corresponding sound channel according to depth. A couple of rays traveled at a depth of about 6 m in the May data. However, these rays were ignored as they diminish in the range-dependent ray simulation due to their sensitivity.

3 Sound transmission data and error evaluation

The sound transmission was sporadically interrupted by environmental factors such as the hulls of ships, surface waves and coastal fronts. More data were missing from the data set for T2 than from that for T1. This is because the bottom topography constructs gentle slopes around T1, in contrast to the sudden deepening seen around T2. This asymmetric bottom topography causes traveling sounds to convergence toward T1 but suddenly spread near T2.

The correlation waveforms obtained at T1 during 11:00–13:00 on March 28, 2010, are shown (as an example of a typical case) with a stack diagram in Fig. 4a in such a way that the transmission time is progressed upward.

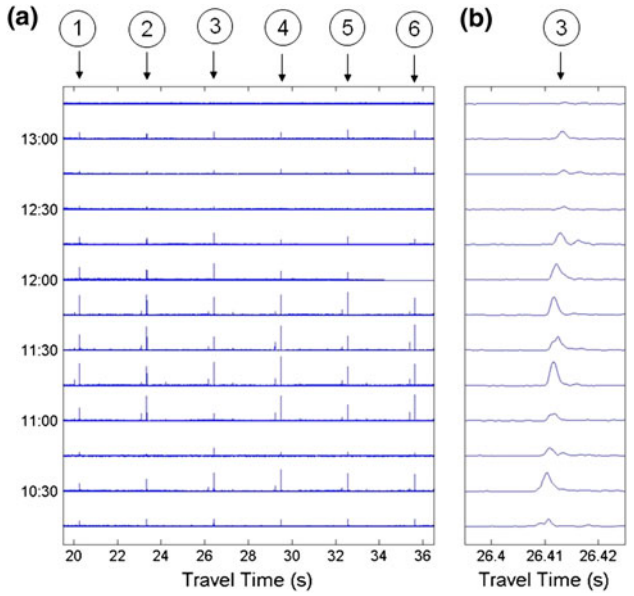

Fig. 4 Stack diagram of the correlation waveforms for the six M-sequence periods of sound received, obtained at T1 during 11:00–13:00 on March 28, 2010 (**a**). The data for the third period of sound received are magnified in **b**. The order that the repeated sounds were received is indicated by the *circled numbers* above the plots

The correlation peak height varies considerably with not only the repeat number (horizontal axis) but also the transmission time (vertical axis). The peaks for the third period of sound received tended to have the greatest heights. Thus, the correlation waveforms for the third period of sound received are magnified in Fig. 4b. The travel times were determined for the maximum peak point in each correlation waveform. Only peak points with signal-to-noise ratios (SNRs) >7 (equivalent to dB = 20 log (7) = 16.9) are considered in the following travel time analyses.

The range-averaged current can be estimated only for periods for which the reciprocal (travel time difference) data were successfully acquired. The error bar for short-term current measurement can be evaluated based on the STD from the mean current, which was calculated from the data for the six repeated periods of sound received. The STDs for the currents are shown in the time plots of Fig. 5. Continuous data were successfully acquired during the March 25–April 16 period (period 1) and the April 22–May 5 period (period 2). The STDs are scattered across the region of <6 cm/s, and have mean values of 1.8 cm/s for period 1 and 1.7 cm/s for period 2. These values are significantly smaller than the average current values of 3.8 and 4.4 cm/s during the two periods, as shown in Fig. 6.

The error bar for short-term temperature measurements can also be obtained from the STD from the mean temperature, as calculated from the data for the six repeated periods of sound received. The STDs for temperature are shown in the time plots of Fig. 7a, b for T1 and T2, respectively. They are scattered across the region of <0.05°C and have mean values of 0.007 and 0.006°C for T1 and T2, respectively. These values are small enough to perform the accurate measurement of temperature.

The range-averaged speed of sound can be estimated from not only the reciprocal data (mean travel times) but also the one-way travel-time data. When the one-way method is used, the effect of current becomes a source of error in speed of sound estimates. The first error (i.e., the effect of current) is diminished when the mean travel time is calculated using the reciprocal travel-time data. This error bar was found to be 0.05°C for the maximum diurnal tidal current, as shown for the typical case of Fig. 8. The temperature was estimated by converting from the speed of sound, using the standard speed of sound formula (Mackenzie 1981). Here, two more error sources (salinity and depth) arise in the conversion. The second error (i.e., the effect of salinity) is caused by its deviation from the reference value. During the experimental period, the range-averaged salinity varied from 33.0 in March to 33.2 in May. This salinity deviation causes a temperature shift of 0.07°C for a fixed speed of sound (1493 m/s) and a fixed depth (10 m) for March. The third source of error comes from the range of depths at which the sound travels. According to the range-independent ray simulation results in Fig. 3, the depth ranges for the traveling rays are 0–20 m for March and 10–25 m for May. The difference between the mean depths for these months (7.5 m) causes a temperature shift of 0.04°C for a fixed speed of sound ($C = 1493$ m/s) and a fixed salinity ($S = 33.0$) for March. However, these second and third errors can be diminished by updating the salinity and depth values prior to the conversion from the speed of sound into temperature.

4 Temporal variations in current and temperature

The range-averaged current was calculated from the travel-time difference data obtained during the successful acquisition of reciprocal data (Fig. 6). Significant semidiurnal and fortnightly variations were visible, although there were large amounts of missing data during March 16–24 and April 17–22. The amplitude of the fortnightly variation was over 30 cm/s, with slightly larger positive values. The along-line mean currents calculated for the two 13.66-day periods during March 25–April 7 (period 1) and April 23–May 6 (period 2) were 3.8 and 4.4 cm/s, respectively, referring to the direction from T1 to T2. The STDs (error bars) for current variations were 1.8 cm/s for period 1 and 1.7 cm/s period 2, and are indicated by thick vertical bars in the figure.

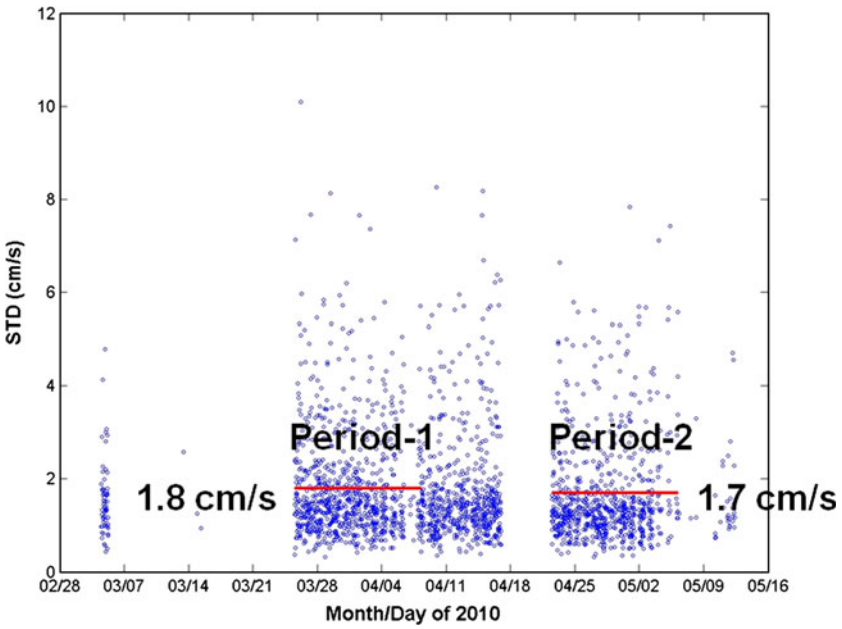

Fig. 5 STD versus time for current variations, calculated every 15 min from the data for the six repeated periods of sound received. The *thick horizontal lines* show the mean STDs for period 1 and period 2

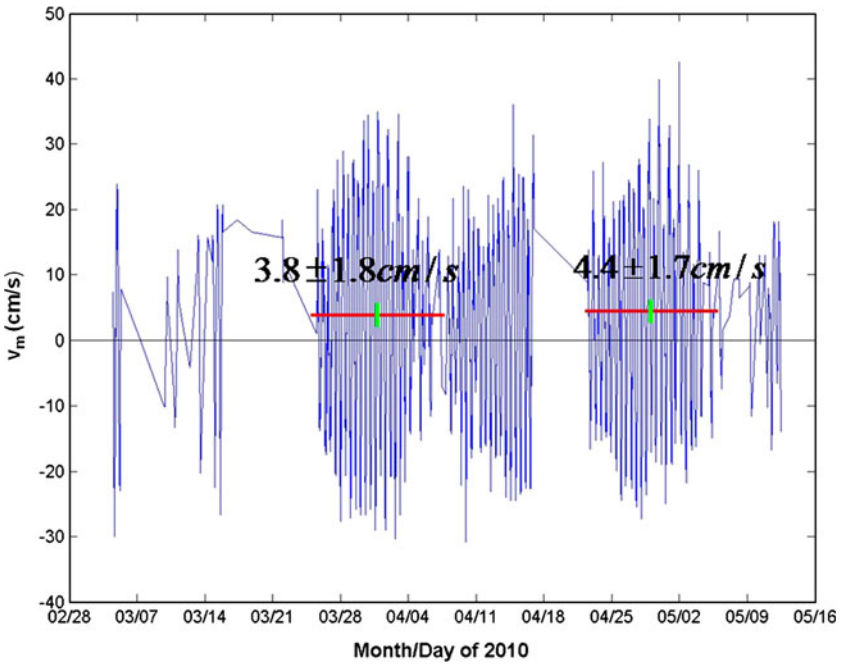

Fig. 6 Time plot of the range-averaged current for the whole observation period, calculated from travel-time differences. The *thick horizontal and vertical bars* show the mean and its STD calculated for periods 1 and 2, respectively

The range-averaged temperature was calculated from the mean travel-time data or one-way travel-time data. Three kinds of temperatures (two one-way data sets and one reciprocal data set) were obtained during the successful acquisition of the reciprocal data (Fig. 8). The tidal gauge data at Matsuyama and the current data from the reciprocal transmission for the same period are also shown in the upper and middle panels of the figure, respectively. The effect of current to temperature variation is around 0.05°C. A prominent semidiurnal variation in temperature is the strongest feature of the figure. Upon comparing these figures, when there is no effect of current, the temperature (blue line) increases during the flood tide (eastward tidal current), while this tendency reverses during the ebb tide (westward tidal current). During the flood tide with the along-line current component directed from T1 to T2, the temperature is underestimated for one-way data obtained at T1 (green line) and overestimated for one-way data obtained at T2 (red line). The effect of the tidal current on the temperature reverses during the ebb tide when the along-line current component is directed from T2 to T1. It is worth noting that the eastward and westward tidal

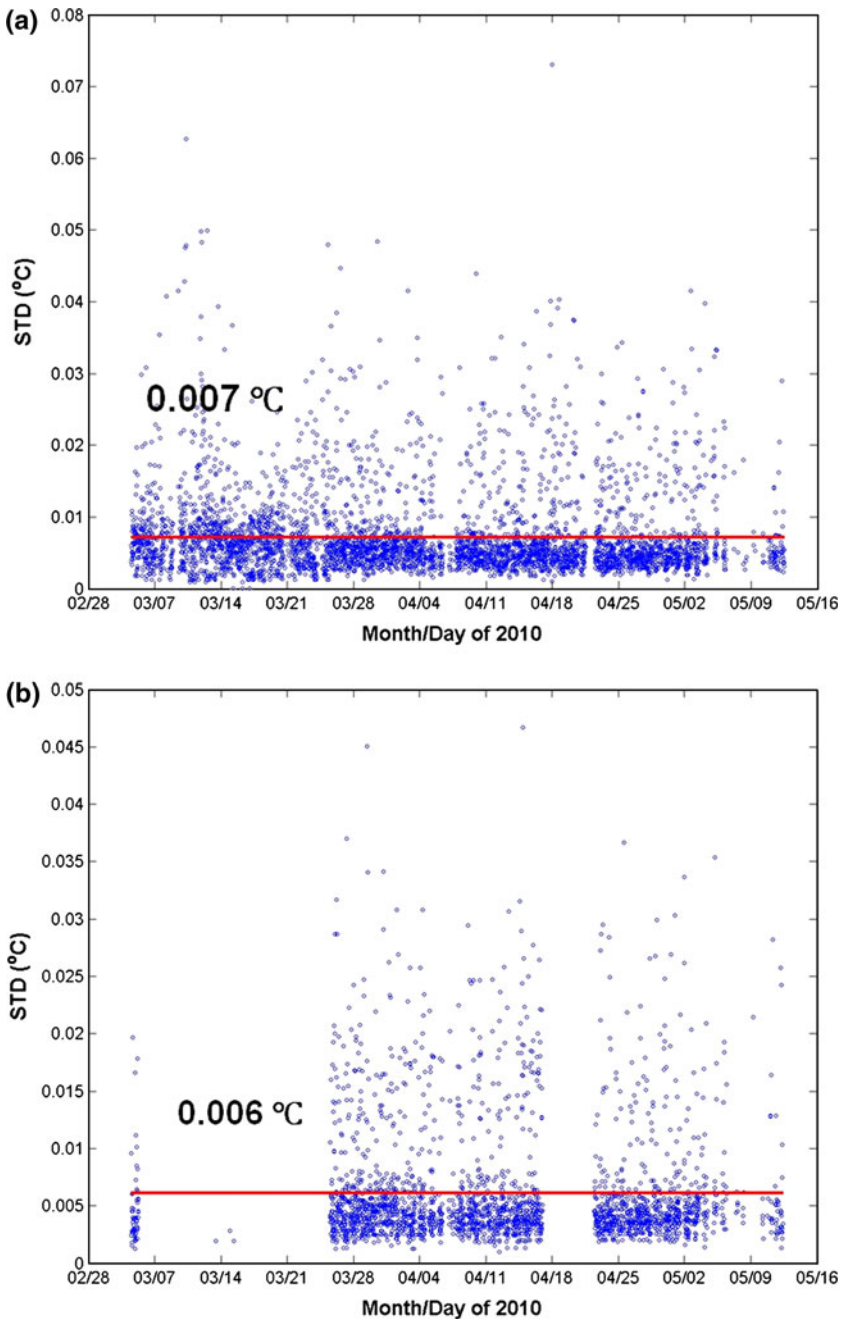

Fig. 7 Time plots of the STD in the temperature variation at **a** T1 and **b** T2, as calculated every 15 min from the data for the six repeated periods of sound received. The *thick horizontal line* shows the mean STD for the whole observation period

currents, which occurring in phase with the tides in Aki-nada, correspond closely to the positive and negative along-line currents in the reciprocal transmission experiment, respectively.

The length (L_t) of the tidal excursion for the semi-diurnal tide during the spring tide can be expressed by

$$L_t = \frac{V_{M2} T_{M2}}{\pi}, \tag{5}$$

where V_{M2} is the amplitude of the M2 tidal current in the east–west direction and T_{M2} is the period of the M2 tide. Upon substituting $V_{M2} = 0.3$ m/s for the spring tide and $T_{M2} = 12.42$ h into Eq. 5, L_t drops to about 4.27 km. The peak-to-peak range of temperature variation of 0.17°C provides an east–west temperature gradient of 0.17°C/4.27 km (0.40°C/10 km). The eastward decrease in the sea surface temperature is usually visible in overviews from satellite SST images of the Seto Inland Sea, although the accuracy of the satellite measurements is insufficient to be able to quantify the rate of eastward decrease in temperature.

The temperature data obtained at T1 and T2 at 15-min intervals are shown in the time plots of Fig. 9a, where linear interpolation has been performed to account for

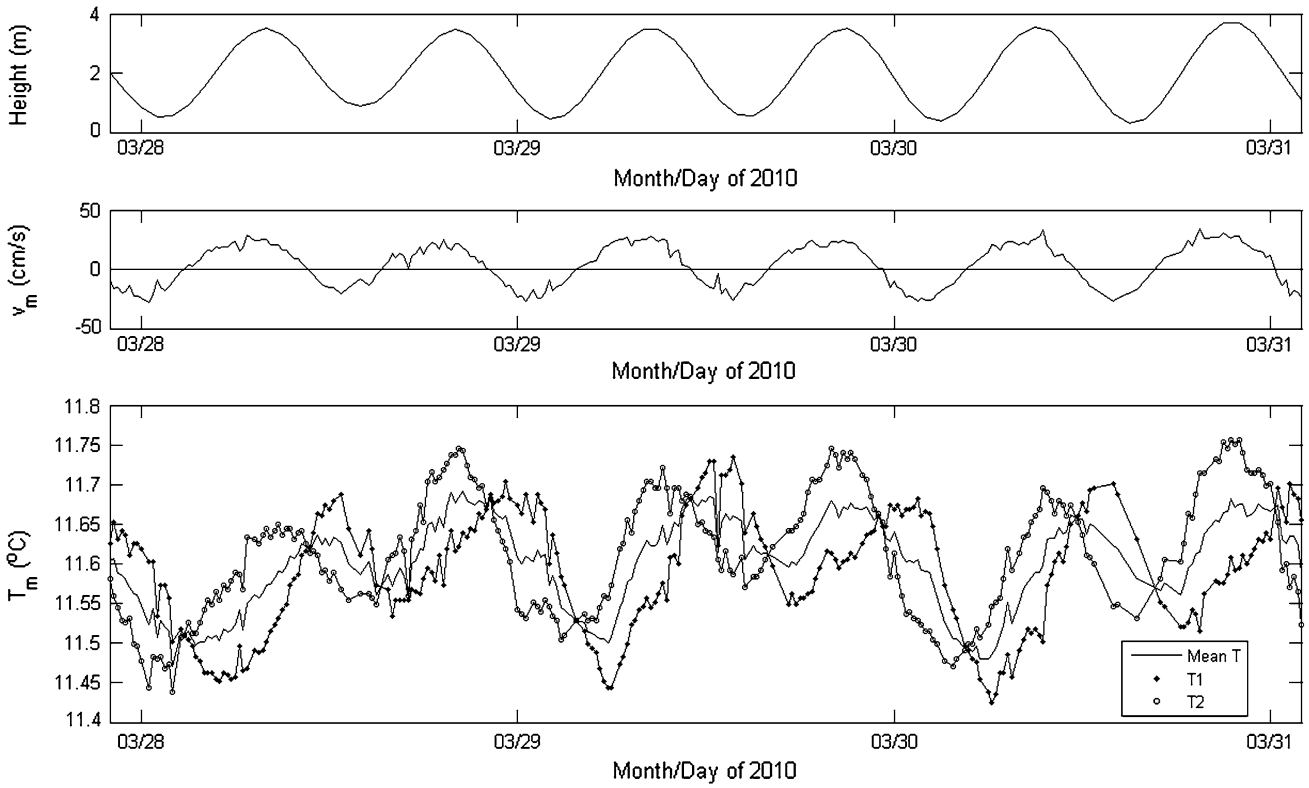

Fig. 8 Time plots of the range-averaged temperature during March 28–30, when the reciprocal data were acquired. The temperature variations in two one-way data sets (*line with circles* for T1 and *line with dots* for T2) and one reciprocal data set (*solid line*) are shown in the *bottom* figure. The tidal gauge data at Matsuyama and the current data from the reciprocal transmission for the same period are also shown in the *upper* and *middle panels* of the figure, respectively

missing data. The CTD temperatures acquired in March and May are plotted as solid circles in the figure, and these show good agreement with the sound transmission temperature. The difference between the T1 data (with less missing data) and the CTD data is 0.07°C for the March data and 0.05°C for the May data. The seasonal warming at a timescale of >30 days was subtracted from the 15-min interval data, and the resulting high-pass-filtered data are shown in Fig. 9b. Here, a weak 10–20 day fluctuation in the range of ±0.2°C can be seen together with the fluctuations due to semidiurnal and diurnal tides.

The specific timescales for the temperature variation were then evaluated quantitatively by power spectral density analysis, and the results are shown in Fig. 10, together with the 95% confidence interval. Besides the features corresponding to semidiurnal and diurnal tides, significant spectral peaks are visible at 7.0 and 21.1 days.

5 Summary and discussion

Current and temperature measurements achieved using long-range reciprocal sound transmission were obtained for the first time for the Seto Inland Sea. The mean current and temperature variations in the central part of the Seto Inland Sea (Aki-nada) were successfully measured during March–May 2010 using a 30 km range reciprocal sound transmission experiment between Honshu and Shikoku. The short-term accuracies of the current and temperature measurements were examined by gauging the STD for the data received for six repeated periods of sound lasting 18.43 s. The accuracy of the temperature measurements were also validated by comparison with the CTD data acquired during the sound transmission experiment.

The range-averaged mean currents calculated along the sound transmission line were 3.8 and 4.4 cm/s for the two 13.66-day periods (periods 1 and 2), respectively, and these values were greater than the STDs (error bars) of 1.7–1.8 cm/s. It can thus be concluded that the positive current (directed toward T2 from T1) reaches a significant level. This positive along-line current points to an eastward current rather than a westward current through Aki-nada.

On the other hand, the short-term accuracy of temperature measurements was estimated to be less than 0.01°C, using the reciprocal transmission data. The effects of salinity and depth as other error sources were greatly reduced when the salinity and depth were updated using newly acquired CTD data at appropriate intervals during

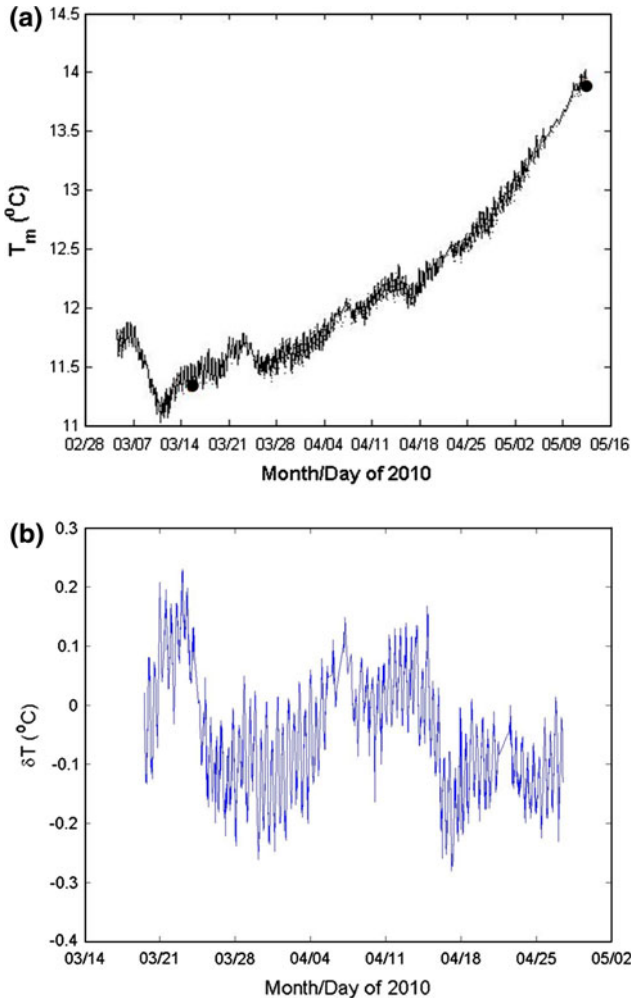

Fig. 9 **a** Time plot of the range-averaged temperatures for T1 (*solid line*) and T2 (*dashed line*), where linear interpolation has been performed to account for missing data. The *dots* show the CTD data obtained on March 15 and May 12. High-pass-filtered data obtained by subtracting the 30-day running mean data from the original data obtained at 15-min intervals are shown in **b**

the sound transmission experiment. This high accuracy of the temperature measurements was also supported by the finding that the temperature differences between the sound transmission and the CTD data were as small as 0.07°C for the March data and 0.05°C for the May data.

Temperature variations with 7.0- and 21.1-day periods were found in the power spectral density diagram with a 95% confidence interval. These peaks in temperature have never been reported previously for Aki-nada, which may be partly due to their weak energies. It should be noted that relatively weak temperature variations in the range of ±0.2°C can only be correctly measured using the long-range sound transmission technique. The typical periods of the temperature variations mentioned above are close to the periods of the Kyucho, implying a connectivity between

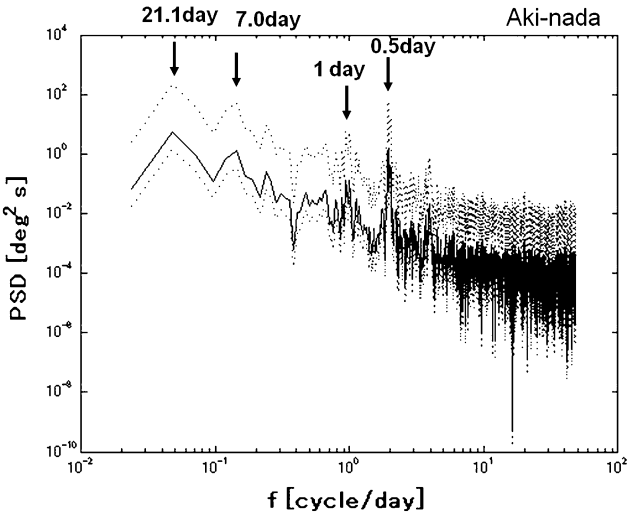

Fig. 10 Power spectral density diagram for the interpolated temperature data, processed through a 30-day high-pass filter. The periods for the significant spectral peaks are indicated with *downward arrows* above the corresponding peaks. The *dashed lines above and below the spectral line* shows 95% confidence intervals

the Bungo Channel and Aki-nada (Akiyama and Saitoh 1993).

This study suggests that reciprocal sound transmission is a powerful technique for the long-term and accurate measurement of mean current and temperature variations in coastal and inland seas.

Acknowledgments Dr. Yoshio Takasugi is greatly acknowledged for his kind support in relation to the instrumentation. This study was supported by grants from the Japan Society for the Promotion of Science and the Dean of the Graduate School of Engineering, Hiroshima University.

References

Akiyama H, Saitoh S (1993) The Kyucho in Sukumo Bay induced by Kuroshio warm filament intrusion. J Oceanogr 49:667–682

Arai M (2004) Development of a semi-spectral coastal ocean model and its application to the Neko Seto Sea in the Seto Inland Sea. J Oceanogr 60:597–611

Chang P, Guo X, Takeoka H (2009) A numerical study of the seasonal circulation in the Seto Inland Sea, Japan. J Oceanogr 65:721–736

Guo X, Futamura A, Takeoka H (2004) Residual currents in a semi-enclosed bay of the Seto Inland Sea, Japan. J Geophys Res 109:C12008. doi:10.1029/2003JC002203

Kaneko A, Yamaguchi K, Yamamoto T et al (2005) A coastal acoustic tomography experiment in Tokyo Bay. Acta Oceanologica Sinica 24(1):86–94

Komai K, Hibino T, Ohkama T (2008a) Influence of the Kuroshio Meander/straight on flow in the Seto Inland Sea. Proc Jpn Soc Civ Eng 63(3):165–179

Komai K, Kim K, Ikehara K et al (2008b) Annual variation of throughflow in the Seto Inland Sea. Coast Eng Jpn 55:406–410 (in Japanese with English abstract)

Kunii M, Fujiwara T (2006) Through flow of the Seto Inland Sea driven by the sea level difference between western and eastern boundaries. Umi-to-Sora 81(2):13–21 (in Japanese with English abstract)

Lin J, Kaneko A, Gohda N et al (2005) Accurate imaging and prediction of Kanmon Strait tidal current structures by the coastal acoustic tomography data. Geophys Res Letts 32:L14607. doi:10.1029/2005GL022914

Mackenzie KV (1981) Nine-term equation for sound speed in the ocean. J Acoust Soc Am 70:807–812

Munk W, Worcestor PF, Wunsch C (1995) Ocean acoustic tomography. Cambridge University Press, Cambridge

Nguyen H, Kaneko A, Lin J et al (2009) Acoustic measurement of multi sub-tidal internal modes generated in Hiroshima Bay, Japan. IEEE J Ocean Eng 34(2):103–112

Park JH, Kaneko A (2000) Assimilation of coastal acoustic tomography data into a barotropic ocean model. Geophys Res Letts 27(20):3373–3376

Takasugi Y, Hoshika A, Noguchi H et al (1994a) The role of tidal vortices in the material transport around straits. J Oceanogr 50:65–80

Takasugi Y, Fujiwara T, Sugimoto T (1994b) Formation of sand banks due to tidal vortices around straits. J Oceanogr 50:81–98

Takeoka H, Akiyama H, Kikuchi T (1993) The Kyucho in the Bungo Channel, Japan–Periodic intrusion of oceanic warm water. J Oceanogr 49:369–382

Takeuchi J, Honda N, Morikawa Y et al (1998) Bifurcation Current along the southwest coast of the Kii Peninsula. J Oceanogr 54:45–52

Yamaguchi K, Lin J, Kaneko A et al (2005) A continuous mapping of tidal current structures in the Kanmon Strait. J Oceanogr 61:283–294

Yanagi T, Higuchi H (1979) Constant flows in the Seto Inland Sea. Bull Coast Oceanogr 16:123–127